Cardiovascular Engineering and Technology, Vol. 3, No. 2, June 2012 *(© 2012)* pp. 171–178
DOI: 10.1007/s13239-012-0090-x

Dispersive Transport of Angiographic Contrast During Antegrade Arterial Injection

QING HAO[1] and BARUCH B. LIEBER[2]

[1]Biotechnology and Bioengineering Center, Medical College of Wisconsin, Milwaukee, WI, USA; and [2]Department of Neurosurgery, State University of New York, Stony Brook, NY, USA

(Received 10 January 2012; accepted 29 March 2012; published online 13 April 2012)

Associate Editor Keefe B. Manning oversaw the review of this article.

Abstract—Angiography is commonly used during endovascular procedures to navigate catheters into a target artery and for evaluation of the arterial luminal geometry. X-ray attenuating contrast material is injected into the arteries and transported into pathologies such as aneurysms or arteriovenous malformations. Images of the transported contrast are used to guide therapeutic decisions. Experience and intuition of the interventionalist are often serving as guide for the injection force, and hence, the speed and volume of the bolus. Forceful injections of small boluses can evoke local turbulence and dispersive mixing in the zone immediately distal to the catheter tip. Turbulence by its nature acts as a strong agitating mechanism such that the bolus of contrast quickly mixes with the flowing blood to occupy the entire lumen so the artery can be visualized. The aims of the present study are (a) to determine the distance from catheter tip beyond which contrast can consider to be fully mixed with the blood during antegrade injection and (b) to determine the thickness of the boundary layer in which contrast concentration is poor, which can contribute to underestimation of vascular diameter using this method. We performed *in silico* experiments to describe blood and angiographic contrast transport in a straight artery model. The conditions investigated are derived from clinical contrast injection rates typically found in cerebral angiography. A recirculation flow exists in the mixing zone distal to the catheter tip issuing the contrast and convective mixing rather than diffusion is dominating the rapid mixing process. In the vicinity of the arterial wall in the mass transfer boundary layer, however, transport is dominated by molecular diffusion. For lower molecule diffusion coefficient, the mass transfer boundary layer contains a lower concentration of contrast than for a higher molecular diffusion coefficient. These findings imply that contrast visibility near the arterial wall is poor such that arterial dimensions derived from angiograms may be underestimated and consequently sizing of potential implants inaccurate. Outside the mass transfer boundary layer contrast can be considered as fully mixed with the carrying flow in about 10 arterial diameters distal to the injection port.

Address correspondence to Baruch B. Lieber, Department of Neurosurgery, State University of New York, Stony Brook, NY, USA. Electronic mail: baruch.lieber@sbumed.org

Keywords—Computational fluid dynamics (CFD), Dispersive mixing, Mass transfer, Contrast injection, Turbulence.

INTRODUCTION

Angiography guided endovascular procedure requires percutaneous access to the vascular system and injection of contrast material into the blood vessel to attenuate the X-ray beam passing through it. The image receptor is then able to record vascular luminal morphology with high spatial and temporal resolution within a region of interest (ROI) for diagnosis of vascular pathologies. The combined spatial and temporal resolution of angiography allows the operator to see a real-time view of catheters placed in arteries or veins and to navigate the catheters to remote territories under real-time fluoroscopic guidance by superposing a static two- or three dimensional image of the vascular tree (customarily called the roadmap) on the real-time image.[5]

The relationship between the dispersive transport of the contrast and the flowing blood is a highly nonlinear process. Still images are very valuable to provide vascular dimensions, however, observations on contrast transport remain largely qualitative in nature. We examined experimentally the transport of contrast injected into a tube using high speed angiography.[6] We found that under typical coaxial antegrade arterial injection rates, which are customary in the cerebrovasculature, angiographic contrast completely mixes with a blood analog fluid under steady flow conditions within about eight tube diameters downstream of the injection site. In this study we employ a computational flow dynamic model to further elucidate the convective transport of contrast and investigate the extent of the mass transfer boundary layer in a model of a straight artery with a coaxial catheter. Contrast is injected

antegradely into the flowing blood forming a binary mixture under flow condition as in our previous investigation. The results of this investigation compare very well with our experimental results and in addition highlight the significance of the contrast poor boundary layer in estimation of luminal vascular dimensions.

COMPUTATIONAL METHODS

In this study iodinated liquid that commonly serves as a contrast medium during X-ray angiography is continuously injected antegradely into a straight tube ($D = 6.35$ mm) for 2 s through a concentrically placed catheter tip ($d = 2.5$ mm and wall thickness of 0.25 mm) (Fig. 1). The entrance length proximal to the catheter tip, x0, is 9 cm. The flow conditions investigated here match our previous experimental investigation that used an aqueous glycerol fluid to represent blood and a contrast saline mixture. The volumetric flow ratio is representative of injections commonly used in clinical applications. The geometrical dimensions and flow conditions are scaled up to increase spatial resolution but the Reynolds number is maintained to match typical flood flow and contrast injection rates used in cerebral angiography. The properties of the blood analog fluid and the contrast are given in Table 1. The conservation of mass equation, Reynolds averaged Navier–Stokes equations (RANS), convection–diffusion equation, and low Reynolds number (LRN) shear stress transport (SST) κ-ω model are implemented in a CFD package (Fluent 12.1, Ansys Inc., Lebanon, NH) to solve the velocity and distribution of species fields. The problem is formulated as axisymmetric transient Newtonian fluid model. Inlet flow rates used in the simulations are listed in Table 2 together with calculated values of the Reynolds number and the Craya-Curtet number, which is the ratio of the momentum fluxes of the coaxial streams.[2,6] More detailed information on the impact of the Craya-Curtet number on the flow field distal to the catheter tip can be found in the Appendix of Lieber *et al.*[6] The strategy of the solution assumes that the blood flow prior to ontrast injection is steady. The solution of the blood flow field prior to contrast injection is used as initial condition at commencement of contrast injection. The flow field that develops during contrast injection is then solved as a transient problem. Results are succinctly reported during the end of 2 s of contrast injection.

TURBULENCE MODEL

The RANS equations depict transport of only the mean flow quantities while all the turbulent eddies are modeled. In time dependent simulations, the time step is determined by the global unsteadiness in the mean flow, rather than by the turbulence.[16]

In turbulent flows, instantaneous flow variables in the Navier–Stokes equations such as axial velocity, u, can be expressed in terms of an ensemble-averaged quantity $\bar{u}$, and a fluctuation as a departure from this average, u' (and similarly for other scalar quantities

TABLE 1. Properties of glycerol and contrast.

	Density (kg/m^3)	Viscosity (poise)
Glycerol	1098	0.035
Contrast	1170	0.009

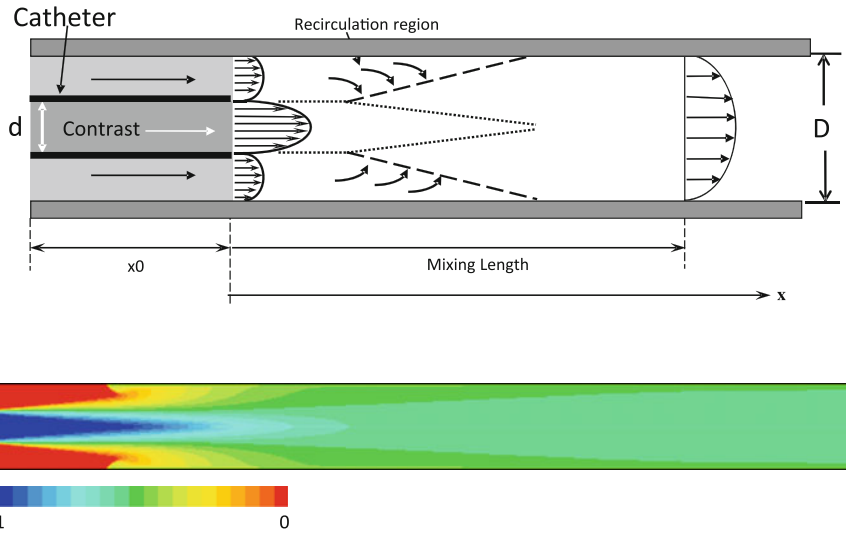

FIGURE 1. Top Panel: Schematic of the flow domain. Bottom panel: Contrast distribution in the flow domain and scale bar showing contrast concentration fraction.

TABLE 2. Flow rates of the contrast and the blood analog fluid used in the computational runs.

Case	Glycerol flow rate (cc/s)	Contrast flow rate (cc/s)	Re (glycerol)	Re (contrast)	Craya-Curtet
1	7	8	567	2270	0.38
2	6.6	7.6	534	2157	0.37
3	6.6	6.9	534	1958	0.44

Note: The values used for the flow rates and tube are the same as in our previous experiments[6] These values are scaled up compare to the size of the arteries *in vivo* to preserve the Reynolds number.

like pressure, concentration, *etc.*). Applying this decomposition to the Navier–Stokes equations yields the RANS equations. The incompressible form of these equations can be written in the Cartesian Einstein Summation convention form with i and j subscripts as:

$$\frac{\partial(\rho\bar{u}_i)}{\partial x_i} = 0 \tag{1}$$

$$\frac{\mathcal{D}(\rho\bar{u}_i)}{\mathcal{D}t} = -\frac{\partial\bar{p}}{\partial x_i} + \frac{\partial}{\partial x_j}\left[\mu\left(\frac{\partial\bar{u}_i}{\partial x_j} + \frac{\partial\bar{u}_j}{\partial x_i}\right)\right] - \frac{\partial}{\partial x_j}\left(\rho\overline{u_i'u_j'}\right) \tag{2}$$

and the contrast concentration transport equation is:

$$\frac{\mathcal{D}c_c}{\mathcal{D}t} = \frac{\partial}{\partial x_i}\cdot\left(\frac{\partial(D_{\mathrm{m}}c_c)}{\partial x_i}\right) \tag{3}$$

Here D_{m} is the molecular diffusion coefficient and c_c is the concentration of the solute (i.e., contrast). $\mathcal{D}/\mathcal{D}t$ is the substantial derivative, μ is dynamic viscosity, ρ is density, p is pressure and $\overline{\rho u_i'u_j'}$ are the usual Reynolds stress tensor terms representing the time-averaged rate of momentum transfer due to turbulence.[17] Expressed in terms of the kinematic eddy viscosity, ν_T, and the mean strain rate tensor, S_{ij} the Reynolds stress tensor takes the form:

$$-\overline{u_i'u_j'} = \tau_{ij} = \nu_T\left(\frac{\partial\overline{u_i}}{\partial x_j} + \frac{\partial\overline{u_j}}{\partial x_i}\right) = 2\nu_T S_{ij} \tag{4}$$

A turbulence model is commonly used to aid in solving the equations due to the highly nonlinear nature of the cross correlations that arise (e.g., the Reynolds stresses) in the governing equations and thereby provide 'closure' to the equations. There are various turbulence models in practice and a particular model is chosen depending on the specific fluid flow applications and physical characteristics. The LRN SST $k-\omega$ model has demonstrated to have excellent performance for wall bounded flows at LRNs. Briefly, in flows under severe adverse pressure gradient (such as the backward facing step), Menter[7] redefined the eddy viscosity to be the transport of the principal turbulent shear stress away from the wall and blended the $k-\varepsilon$ and $k-\omega$ models in such a way that the former is activated away from the wall and reduces to the latter close to the wall. The resulting SST model significantly improves the prediction of flows involving adverse pressure gradients, especially due to its ability to account for transport of turbulent shear stress. More details on all of the models discussed briefly herein can be found in books on turbulent flows and their modeling.[4,10,15,17]

The model uses additional transport equations for turbulent kinetic energy (TKE), k, and specific dissipation rate, ω. The turbulent transport equations for the TKE are:

$$\frac{\mathcal{D}k}{\mathcal{D}t} = \tau_{ij}\frac{\partial\overline{u_i}}{\partial x_j} - \hat{\mathcal{D}} + \frac{\partial}{\partial x_j}\left[\Gamma_k\frac{\partial k}{\partial x_j}\right] \tag{5}$$

$$\hat{\mathcal{D}} = \beta_0^* f_{\beta^*} k\omega \tag{6}$$

$$\Gamma_k = \nu + \frac{\nu_T}{\sigma_k} \tag{7}$$

$$f_{\beta^*} = \begin{cases} 1 & \chi_k \le 0 \\ \frac{1+680\chi_k^2}{1+400\chi_k^2} & \chi_k > 0 \end{cases} \qquad \chi_k \equiv \frac{1}{\omega^3}\frac{\partial k}{\partial x_j}\frac{\partial\omega}{\partial x_j} \tag{8}$$

and the transport equation for ω is:

$$\frac{\mathcal{D}\omega}{\mathcal{D}t} = \alpha\frac{\omega}{k}\tau_{ij}\frac{\partial\overline{u_i}}{\partial x_j} - \beta_0 f_\beta\omega^2 + \frac{\partial}{\partial x_j}\left[\Gamma_\omega\frac{\partial\omega}{\partial x_j}\right], \tag{9}$$

where $\Gamma_\omega = \nu + \frac{\nu_T}{\sigma_\omega}$.

The eddy viscosity for the LRN variation is computed as:

$$\nu_T = \alpha^*\frac{k}{\omega}. \tag{10}$$

The auxiliary relations are described as:

$$\alpha^* = \alpha_\infty^*\left(\frac{\alpha_0^* + \frac{\mathrm{Re}_t}{R_k}}{1 + \frac{Re_t}{R_k}}\right) \tag{11}$$

$$\alpha = \frac{\alpha_\infty}{\alpha^*}\left(\frac{\alpha_0 + \frac{\mathrm{Re}_t}{R_\omega}}{1 + \frac{Re_t}{R_\omega}}\right) \tag{12}$$

TABLE 3. Closure coefficients for the *k*-omega turbulence model.

Model	σ_κ	σ_ω	α^*_∞	R_κ	α_∞	α_0	R_ω	β^*_0	β_0
Low Re κ-ω SST	2.0	2.0	1.0	6.0	0.52	$\frac{1}{9}$	2.95	$\frac{9}{100}$	$\frac{9}{125}$

$$\mathrm{Re}_t = \frac{k}{\nu\omega} \tag{13}$$

$$f_\beta = \frac{1+70\chi_\omega}{1+80\chi_\omega} \tag{14}$$

$$\chi_\omega = \left|\frac{\Omega_{ij}\Omega_{jk}\Omega_{ki}}{(\beta^*_0\omega)^3}\right| \tag{15}$$

$$\Omega_{ij} = \frac{1}{2}\left(\frac{\partial \overline{u_i}}{\partial x_j} - \frac{\partial \overline{u_j}}{\partial x_i}\right). \tag{16}$$

Closure coefficients for this model can be found in Table 3.

NUMERICAL MODELING FOR THE FLOW AND MASS FIELD

The differential equations are discretized using the Semi-Implicit Method for Pressure-Linked Equations (SIMPLE) algorithm.[9] Momentum, turbulence kinetic energy, specific dissipation rate and species are discretized and formulated in first order upwind schemes; the time step is formulated as a first order implicit scheme. The discretized equations are solved in a segregated manner using the SIMPLE algorithm. The grid is generated using a preprocessor, GAMBIT, residing in FLUENT.

No-slip boundary conditions are applied on the vessel wall as well as the inner and outer walls of the catheter. The inlet velocity profile is chosen to be fully developed and coded in Fluent User Defined Function (UDF). The initial condition for the contrast is set such that at the issuing tip of the catheter its relative concentration is 1 and outside the catheter it is zero. The computation time step is set to 0.01 s and the contrast injection lasts for 2 s. The flow field that is established 2 s into the contrast injection is reported in the results section for brevity.

RESULTS

The mass fraction of the mixture downstream of the contrast injection port is shown in Fig. 1. The top panel shows schematically the flow field that ensues in the tube after the start of the contrast injection. A confined jet is established with the core of the jet being carried a few diameters downstream of the catheter tip. The jet is then spreading to occupy the entire arterial lumen creating a recirculation zone in its wake. Blood is entrained into the spreading jet and this entrainment enhances the mixing process. Since the Reynolds number of the flow is not sufficiently high to sustain the turbulence a short distance further downstream the flow reorganizes and returns to laminar. These flow characteristics are reflected in the species concentration as shown in the bottom panel of Fig. 1. At about the same axial location where the core jet of contrast disappears, a flow separation zone near the wall of the tube is evident. Following the separation zone there is a region of enhanced mixing. Further downstream the mixture occupying the tube appears to be completely mixed. A closer examination of the concentration profiles across the tube diameter at various downstream locations is given in the three panels of Fig. 2 for a molecular diffusion coefficient of 5×10^{-9} m^2/s. The hemodynamic and injection rate characteristics for the three panels are given in Table 2. The main changes in the concentration profiles for these conditions are limited to a few diameters ($<$6D) downstream of the catheter tip. Beyond that location axial profiles of the species concentration are quite similar. They appear flat showing a fully mixed condition with changes in concentration that are limited to a thin layer near the wall. It is also worthwhile noting that in the mixing zone, about 6–10 diameters downstream of the jet the concentration of contrast in the wall layer is quite high mainly due to turbulent mixing. Beyond the mixing zone, as the flow reorganizes, the concentration of contrast in the wall boundary layer drops significantly for all three cases.

Figure 3 shows the axial velocity distribution in the tube at different axial locations downstream of the injection port for the hemodynamics of case #1. The velocity distributions are typical for mixing coaxial streams of large velocity discrepancies with the high velocity jet in the center. The profiles show that the jet dissipates within five to six tube diameters downstream of the injection site and further downstream in the far field the velocity profiles are self-similar with an appearance of laminar flow. The bottom panel of Fig. 3 shows the velocity profiles in the near field where mixing takes place. Noteworthy is the recirculation zone near the tube wall between two to three diameters downstream of the contrast entry point. At four diameters downstream the recirculation disappears,

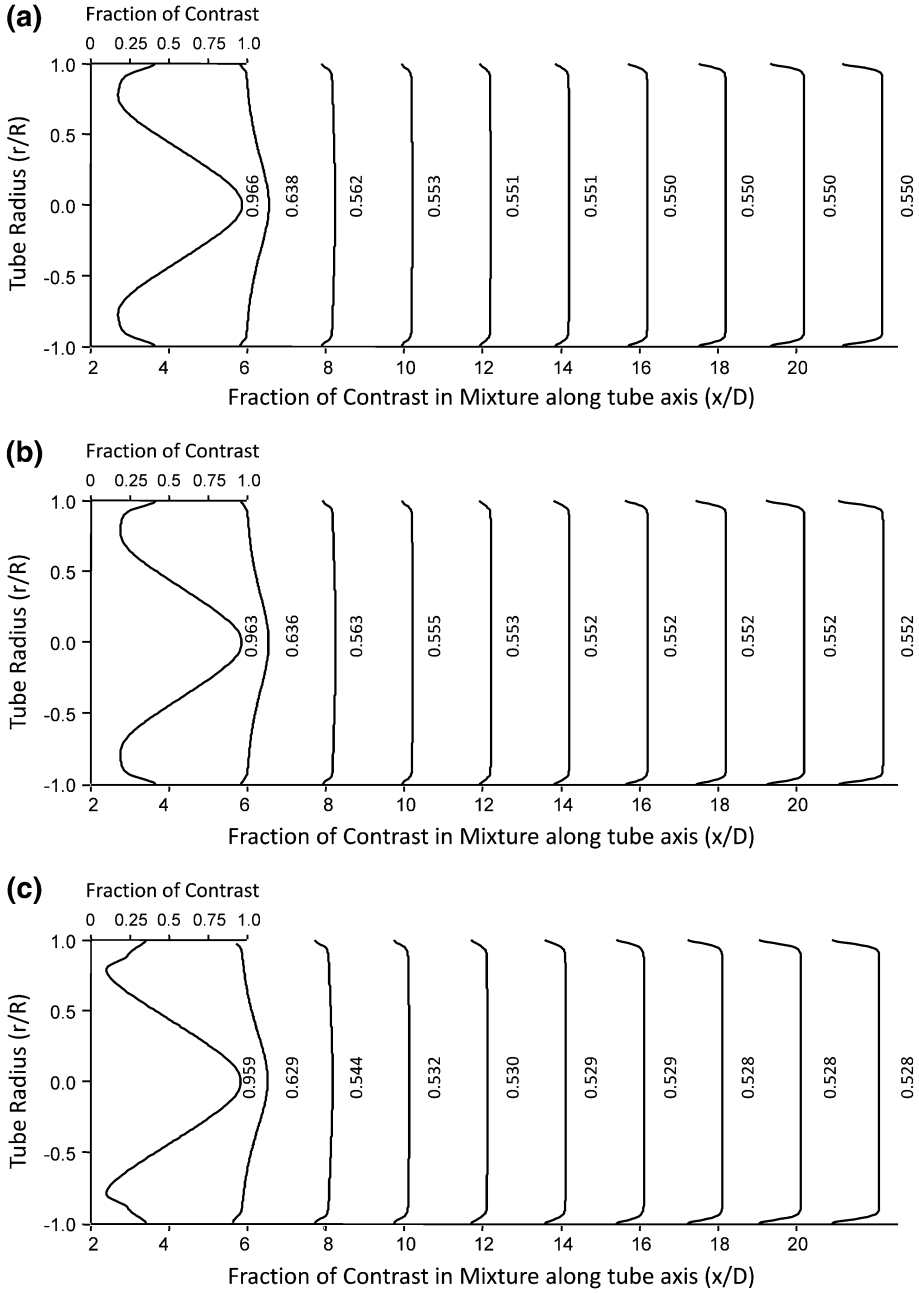

FIGURE 2. Radial distribution of the mass fraction of contrast along the tube axis every 2 tube diameters distal to the injection port (A = Case #1; B = Case#2; C = Case #3). Maximum values are noted in each profile.

although, there is still an inflection point in the profile near the wall. The existence of such a recirculation zone has been investigated extensively in the past[2,3,11–14] and its formation is governed by the Craya-Curtet number.

An estimation of the length of the mixing zone is shown in Fig. 4. The graphs were obtained by taking the root sum of squares of the difference in the concentration profiles successively at each tube diameter distal to the injection port. As can be noted, for the three cases investigated, the function attains a minimum at about 10 diameters distal to the catheter tip signifying minimal changes in concentration profiles at that location compare to previous axial location. The gradual increase in the value of the function beyond the minimum value at 10D is primarily due to reduction in the concentration of contrast in the wall boundary layer in successive profiles beyond that point. This phenomenon is also supported by our investigation of various diffusion coefficient values that is shown in Fig. 5 for the hemodynamic conditions of case #3. Note that near the contrast injection

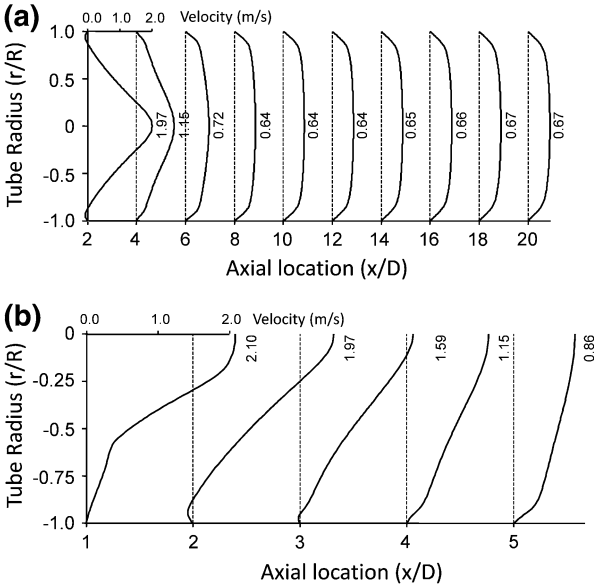

FIGURE 3. Top: Radial distribution of the velocity along the tube axis every 2 tube diameters distal to the injection port (Case #1). Bottom: close up of velocity distribution showing recirculation near the wall. Maximum values are noted in each profile.

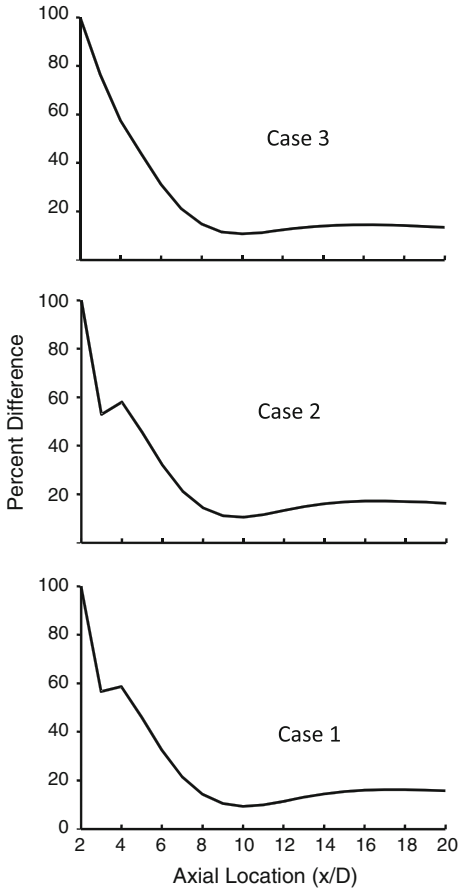

FIGURE 4. Percent difference of the average radial contrast distribution at successive axial locations (Case #1).

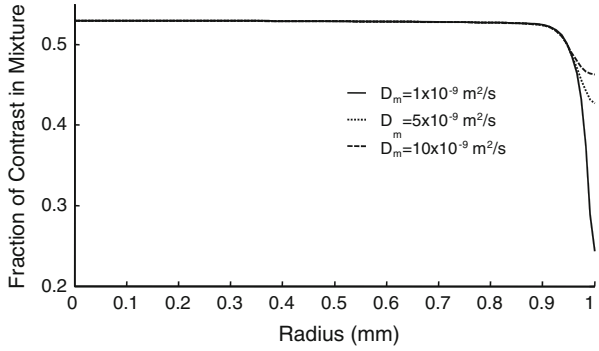

FIGURE 5. Radial distribution of contrast at $x = 10D$ for different molecular diffusion coefficients (Case #3).

port there is a notch in the function due to instability of the jet and hence abrupt changes in the velocity profiles at that location for two of the cases investigated.

Figure 5 shows the fraction of contrast concentration along the radius of the tube at 10 tube diameters downstream of the injection port for three different molecular diffusion coefficients of 1×, 5×, and 10×10^{-9} m^2/s. Outside the wall boundary layer the concentration profiles are flat and nearly identical. This signifies that the mixing process is dominated by convective mixing, not by molecular diffusion and that at this axial location the mixture is homogeneous for all three cases. However, near the wall the concentration of contrast is markedly diminished due to lower near wall fluid velocity; thus, molecular diffusion is dominant at the wall region. For the lowest molecular diffusion coefficient the concentration of contrast near the wall drops sharply compare to the higher molecular diffusion coefficients, although, some difference between the other two diffusion coefficients is also apparent.

DISCUSSION

Angiographic contrast is routinely used during interventional procedures and vascular geometry is assessed from the images for diagnostic and therapeutic purposes. With the advent of flat panel detectors in recent years, replacing image intensifiers, improving the Hounsfield and spatial resolution of cone beam angiography[8] and with rotational capabilities of modern c-arms three dimensional maps of the cerebrovasculature are routinely obtained. Furthermore, the successful implementation of 3-D reconstruction algorithms on modern C-arms prompted their use to produce 3-D maps of the cerebrovasculature. Although still investigational some neuro-interventionalists are increasingly advocating the use of Cone Beam CT (CBCT) instead of Multi Detector CT (MDCT). The impetus for such

advocacy is to shorten the time between the diagnostic and the intervention phase of patient care. Recent evaluations of CBCT reconstruction of 3D vascular geometry vs. MDCT angiography suggests that CBCT produces 3D images of adequate quality to answer the relevant clinical question without transporting the patient.[8]

Increasingly such vascular maps are also exploited in research by adding computational flow solutions to the vasculature. However, most of the scientists that use such vasculature tend to overlook the limitations involved with the obtained vascular maps. One limitation is the lack of small branches that are not opacified enough by contrast for X-ray visualization. Another problem is underestimation of the true caliber of the vessels because the X-ray beam passes through a thinner layer of contrast in the vicinity of the walls due to the circular shape of the arteries as we have shown in our previous study.[6] Here we highlight another limitation of contrast based imaging of the arterial lumens. Poor contrast penetration into the boundary layer near the tube walls exacerbate the poor visibility of near wall arterial lumen. Contrast poor boundary layer thickness estimated in this study occupies about 10% of the tube radius. The thickness of the contrast poor layer is determined, in analogy to the momentum boundary layer thickness of fluid flow applications, where the concentration of the contrast reaches 99% of the free stream. Therefore, vascular caliber as measured from the obtained image may be an underestimation of the true caliber because of the combined issues of thin layer thickness and poor contrast concentration at the same location.

In this study as well as in our previous investigation we used blood and contrast flow rates that are typically employed during an arterial injection particularly in the cerebrovasculature. In the experiments we scaled up the tube and catheter dimensions to obtain better spatial resolution and adjusted the flow rates to match the Reynolds numbers to the *in vivo*, a typical approach in flow dynamics similitude. One limitations of this study is the use of steady flow rather than pulsatile flow. However, since the duration of the injections are much longer than the duration of systole, additional agitation by pulsatility is likely to have a small effect on mixing as we have shown in the carotid of the Rabbit.[6] Another limitation arises from the unknown molecular diffusion coefficient of angiographic contrast. However, the molecular diffusion coefficient of iodine in aqueous solutions has been investigated before and reported to be about 1.36×10^{-9} m^2/s at 298 °K with diffusivity increasing to $4.32\ 10^{-9}$ m^2/s at 358 °K.[1] Therefore, we used a range of values that should, in principle, approximate the coefficient of the various contrast agents. Yet another limitation arises from positioning the distal tip of the catheter for contrast injection concentrically in the tube which is not always the case *in vivo*. Departure from the ideal position may result in somewhat different distribution of contrast concentration in the mixing zone but will likely have a small effect on the length of the mixing zone. In summary, the purpose of this study was two folds. First, we opted to confirm that it is feasible to calculate the mixing zone length in typical cerebrovascular arterial injections and such mixing zone is confined to about ten arterial diameters downstream of the catheter tip. Second, we evaluated the thickness of the contrast poor wall boundary layer and its potential influence on arterial calibers that are derived from contrast enhanced images of arterial lumens.

ACKNOWLEDGMENTS

This study was supported by NIH Grant No. R01 NS045753-05A1 to B.B.L.

REFERENCES

[1]Cantrel, L., R. Chaouche, and J. Chopin-Dumas. Diffusion coefficients of molecular iodine in aqueous solutions. *J. Chem. Eng. Data* 42:216–220, 1997.
[2]Curtet, R. Confined jets and recirculation phenomena with cold air. *Combust. Flame* 2:383–411, 1958.
[3]Forstall, W., and A. H. Shapiro. Momentum and mass transfer in coaxial gas jets. *J. Appl. Mech. Trans. ASME* 72:399–408, 1950.
[4]Hinze, J. O. Turbulence (2nd ed.). New York: McGraw-Hill, 1975.
[5]Lieber, B. B., C. Sadasivan, M. J. Gounis, J. Seong, L. Miskolczi, and A. K. Wakhloo. Functional angiography. *Crit. Rev. Biomed. Eng.* 33(1):1–102, 2005.
[6]Lieber, B. B., C. Sadasivan, Q. Hao, J. Seong, and L. Cesar. The mixability of angiographic contrast with arterial blood. *Med. Phys.* 36(11):5064–5078, 2009.
[7]Menter, F. R. Two-equation eddy-viscosity turbulence models for engineering applications. *AIAA J.* 32(8):1598–1605, 1994.
[8]Orth, R. C., M. J. Wallace, and M. D. Kuo. C-arm cone-beam CT: general principles and technical considerations for use in interventional radiology. *J. Vasc. Interv. Radiol.* 19:814–821, 2008.
[9]Patankar, S. V. Numerical Heat Transfer and Fluid Flow. New York: Taylor & Francis, 1980.
[10]Pope, S. B. Turbulence Flows. Cambridge, UK: Cambridge University Press, 2000.
[11]Razinsky, E., and J. A. Brighton. Confined jet mixing for nonseperating conditions. *J. Basic Eng. ASME Publ.* 93: 333–347, 1971.
[12]Revuelta, A., C. Martinez-Bazan, A. L. Sánchez, and A. Liñán. Laminar Craya–Curtet jets. *Phys. Fluids.* 16:208–211, 2004.
[13]Shapiro, A. H. An investigation of ejector design by analysis and experiment—discussion. *J. Appl. Mech.* 18(1):117, 1951.

[14]Strahle, W. C., and S. G. Lekoudis. Evaluation of data on simple turbulent reacting flows. AFOSR TR-85-0880, 1985.
[15]Tenekes, H., and J. L. Lumley. A First Course in Turbulence. Cambridge, MA: MIT Press, 1972.
[16]Varghese, S. S., and S. H. Frankel. Numerical modeling of pulsatile turbulent flow in stenotic vessels. *J. Biomech. Eng.* 125(4):445–460, 2003.
[17]Wilcox, D. C. Turbulence Modeling for CFD (3rd ed.). La Canada, CA: DCW Industries Inc., 2006.